

## Aberration-corrected STEM Imaging and EELS Mapping of BaTiO<sub>3</sub>/SrTiO<sub>3</sub> Interfacial Defects

HsinWei Wu<sup>1</sup>, Sirong Lu<sup>1</sup>, Patrick Ponath<sup>2</sup>, Toshihiro Aoki<sup>3</sup>, John G. Ekerdt<sup>4</sup>, Alexander A. Demkov<sup>2</sup>, Martha R. McCartney<sup>5</sup> and David J. Smith<sup>5</sup>

- <sup>1</sup>. School of Engineering for Matter, Transport and Energy, Arizona State University, Tempe, AZ
- <sup>2</sup>. Department of Physics, University of Texas at Austin, Austin, TX
- <sup>3</sup>. LeRoy Eyring Center for Solid State Science, Arizona State University, Tempe AZ
- <sup>4</sup>. Department of Chemical Engineering, University of Texas at Austin, Austin, TX
- <sup>5</sup>. Department of Physics, Arizona State University, Tempe, AZ

Barium titanate (BaTiO<sub>3</sub>, or BTO) is highly promising for applications in ferroelectric field-effect transistors (FETs) because of its substantial polarization (0.2 C/m<sup>2</sup>), high permittivity (1200) and room-temperature ferroelectricity (T<sub>C</sub> = 120 °C). Unlike bulk BTO, the properties of BTO thin films are strongly affected by the film thickness, internal strain, and BTO/substrate interface structure, and it is crucial to control the interfacial energy by choosing an appropriate buffer layer or a suitable substrate. In this work, BaTiO<sub>3</sub> (BTO)/ SrTiO<sub>3</sub> (STO) heterostructures were grown by molecular beam epitaxy using Nb:SrTiO<sub>3</sub> (001) substrates. Samples suitable for TEM observation were prepared via mechanical polishing followed by argon-ion-milling at liquid-nitrogen temperature. Aberration-corrected STEM images were recorded using a JEOL ARM 200F operated at 200 keV. The beam convergence angle was set at 20 mrad, and the collection angles were 0-22 mrad for LABF imaging and 90-150 mrad for HAADF imaging. EELS was carried out with a NION UltraSTEM100 operated at 100 keV.

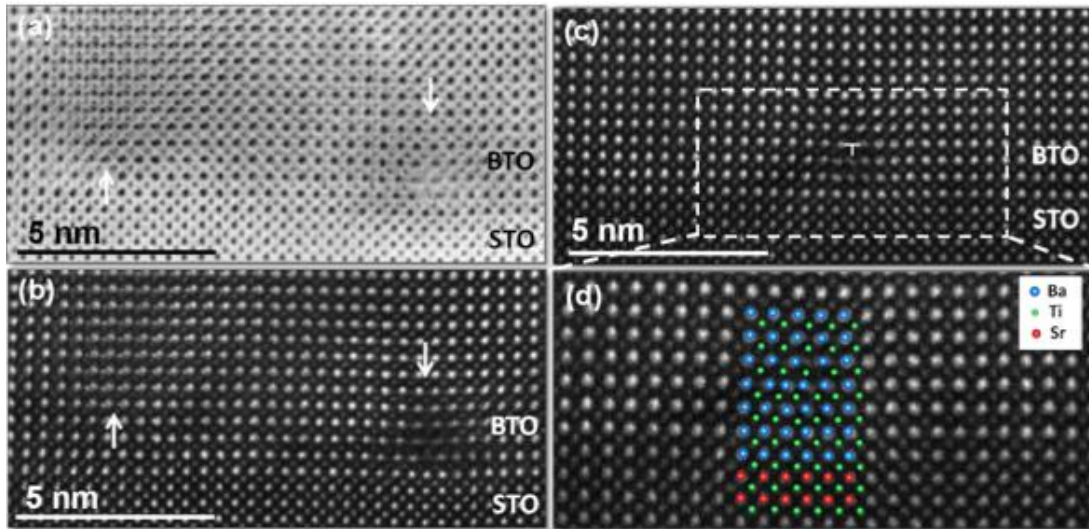
The BaTiO<sub>3</sub> films had an out-of-plane lattice parameter of 4.06 Å corresponding to out-of-plane polarization. However, many <100> misfit dislocations were observed near the BTO/STO interface, as shown in Figs. 1(a) and (b), and anti-phase boundaries were also visible. The offset distances between the dislocation cores and the interface varied considerably between 1 to 5 nm. Figure 1(c) shows another a<100> misfit dislocation located ~2nm away from the BTO/STO interface. Figure 1(d) is a proposed structural model based on the HAADF image, showing a Ba atomic column at the dislocation core. This model closely represents the structure of other misfit dislocations observed in the same sample.

Figure 2 shows elemental EELS mapping acquired from a region of the BTO/STO heterostructure that includes an edge dislocation, with the core located 3 unit cells from the interface. The elemental map indicates no measurable Sr/Ba interdiffusion across the interface or in the region of the dislocation, and is consistent with the proposed crystal structure model shown in Fig. 1(d) with additional Ba and (Ti atomic) columns below the dislocation core. Electron-energy-loss near-edge structure (ELNES) for Ti L<sub>23</sub> edges and O K edges are shown in Figs. 3. These are taken from the STO substrate, marked in red, the edge dislocation, marked in green, and the BTO layer, marked in blue. The BTO and STO show two small satellite peaks in the ELNES spectrum to the right of the Ti L<sub>23</sub> white lines attributed to backscattering from ordered neighboring atoms. When the lattice ordering is broken near the dislocation core, these two peaks are no longer visible, as apparent in Fig. 3 (b). For the O K edges, shown in Fig. 3(c), the peak labeled C, which originates from the nearest O atoms, splits into two smaller peaks, labeled as C1 and C2. This splitting occurs because the crystal structure of the BTO film is tetragonal rather than cubic, breaking the local symmetry. There is no well-defined C peak at the dislocation core

because of the disruption of local ordering, which is similar to results observed from the Ti L<sub>23</sub> edges [1].

References:

[1] This work was supported by AFOSR Contract FA 9550-14-0090. We gratefully acknowledge the use of facilities within the John M. Cowley Center for HREM at Arizona State University.



**Figure 1.** (a) LABF, and (b) HAADF, images showing BaTiO<sub>3</sub>/SrTiO<sub>3</sub> heterostructure with misfit dislocation and anti-phase boundaries. (c) HAADF image of BaTiO<sub>3</sub>/SrTiO<sub>3</sub> misfit dislocation with different offset from interface. (d) enlargement of dislocation core in (c) with proposed crystal structure.

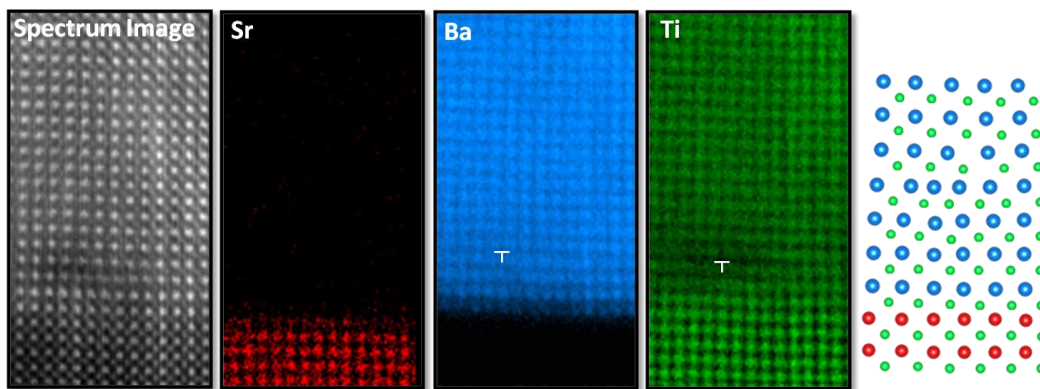


**Figure 2.** Elemental EELS mapping for BaTiO<sub>3</sub>/SrTiO<sub>3</sub> heterostructure with misfit dislocation, confirming no inter-layer diffusion, together with the proposed structural model. The core-less energies for elemental mapping were Sr L<sub>2,3</sub> (1940 eV; 2007 eV), Ti L<sub>2,3</sub> (456 eV, 462 eV), Ba M<sub>4,5</sub> (781 eV, 796 eV), and O K (532 eV).

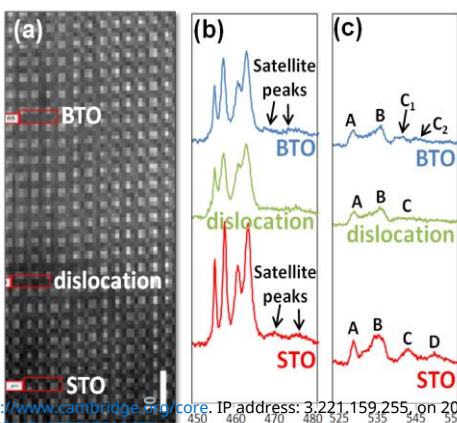


**Figure 3.** (a) HAADF image of BTO/STO heterostructure. Corresponding electron-energy-loss near-edge structure for (b) Ti L<sub>2,3</sub>, and (c) O K edges, for STO substrate, dislocation, and BTO film, as indicated. The core-less energies used for mapping were Ti L<sub>2,3</sub> (456 eV, 462 eV), and O K (532 eV), as indicated.